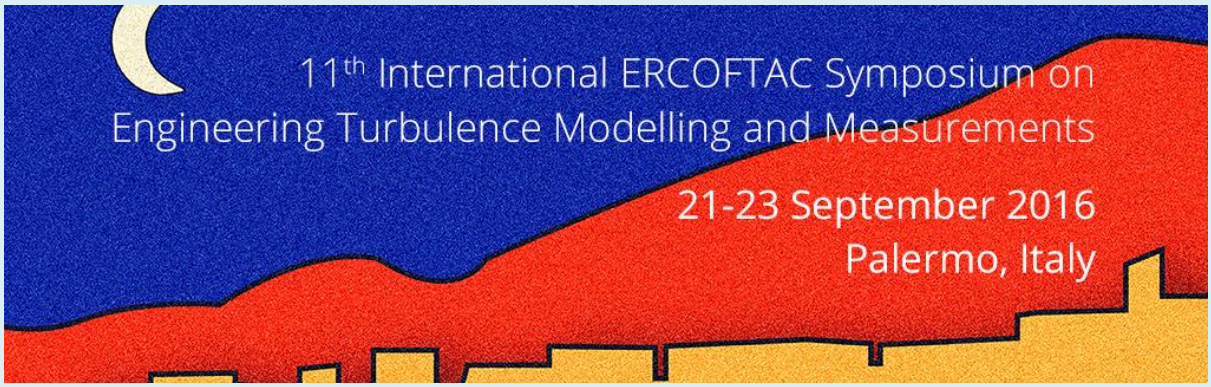

Organizing Committee:

Bernard Geurts (Chairman) - Twente / Eindhoven – the Netherlands

Vincenzo Armenio – University of Trieste – Italy

Ugo Piomelli – Queens University – Kingston – Canada

Donatella Termini – University of Palermo - Italy

Tullio Tucciarelli – University of Palermo – Italy

Enrico Napoli – University of Palermo - Italy

ETMM11 - ERCOFTAC SYMPOSIUM

11th International ERCOFTAC Symposium on
Engineering Turbulence Modelling and Measurements

21-23 September 2016 - Palermo

Program and Full Papers

Notes

You can click on a session in the overview section to view the full details directly

Clicking on a presentation title will open the Full Paper in a new window

---

Organisers

Partners

Coordinator

Overview Programme

Time/Day	Wednesday, 21 September			
	Registration/ Support Desk hours (08:00 - 13:00 & 14:00 - 17:00)			
08:45-09:00	**Welcome and Orientation**			
09:00-09:45	**Karen Flack** (United States Naval Academy) The relationship between surface topography and frictional drag			
09:45-10:30	**Vladimir Nikora** (University of Aberdeen) Turbulence in open-channel flows: recent advances and implications for sediment transport, hydraulic resistance and flow-biota interactions			
10:30-11:00	**Coffee Break**			
11:00-12:40	Hybrid RANS-LES	Particle-laden flow 1	Combustion 1	Wall-bounded flow 1
12:40-14:00	**Lunch**			
14:00-15:40	Wall-bounded flow 2	Particle-laden flow 2	Combustion 2	Experimental fluid mechanics 1
15:40-16:10	**Coffee Break**			
16:10-17:50	DNS for LES	Jet flows	Experimental fluid mechanics 2	Compressible flow
19:00-20:30	**Welcome Reception** Room: Palazzo Sterri (University of Palermo)			

Time/Day	Thursday, 22 September			
	Registration/ Support Desk hours (08:30 - 13:00 & 14:00 - 17:00)			
09:00-09:45	**Simone Hochgreb** (Cambridge) Understanding the structure and dynamics of turbulent reacting flows via selective experiments			
09:45-10:30	**Alfredo Pinelli** (City University of London) Flow manipulation based on passive and localised fluid structure interactions			
10:30-11:00	**Coffee Break**			
11:00-12:40	Flames 1	Manipulated turbulence 1	High fidelity methods 1	Heat Transfer 1
12:40-14:00	**Lunch**			
14:00-15:40	Heat transfer 2	Flames 2	Manipulated turbulence 2	High-fidelity methods 2
15:40-16:10	**Coffee Break**			
16:10-17:50	Turbulence Fundamentals	Bluff body flow	Phase transition	Turbulence-reaction modeling
19:00-22:00	**Conference Dinner** Place: Villa Niscemi			

Time/Day	Friday, 23 September			
	Registration/ Support Desk hours (08:30 - 13:00)			
09:00-09:45	**Sutanu Sarkar** (UCSD) Turbulence at rough topography in the deep ocean			
09:45-10:30	**Detlef Lohse** (University of Twente) Turbulent Rayleigh-Benard and Taylor-Couette flow			
10:30-11:00	**Coffee Break**			
11:00-12:40	Transition	Turbulence models	LES 1	Noise and acoustics
12:40-14:00	**Lunch**			
14:00-15:40	EUROTURBO	LES 2	Friction and drag	Separated flow
15:40-16:00	**Closing address - Announcing ETMM12**			

Thursday, 22 September

09:00-09:45	**Sutanu Sarkar** (UCSD) Turbulence at rough topography in the deep ocean *Chair: Vincenzo Armenio | Room: Normanni*			
09:45-10:30	**Detlef Lohse** (University of Twente) Turbulent Rayleigh-Benard and Taylor-Couette flow *Chair: Donatella Termini | Room: Normanni*			
10:30-11:00	**Coffee Break**			
11:00-12:40	Room: Normanni	Room: Ruggero	Room: Angelica	Room: Basile
	Transition *Chair: Artur Tyliszczak*	**Turbulence models** *Chair: Witold Elsner*	**LES 1** *Chair: Arne Johansson*	**Noise and acoustics** *Chair: Dominic von Terzi*
11:00	On hypersonic boundary layer transition: role of streaks *Jie Ren, Song Fu*	Reappraisal of the constant C_epsilon_2 in the k-epsilon turbulence model *Lyazid Djenidi*	Assessment of subgrid-scale models for large-eddy simulation of complex flows *Franck Nicoud*	Noise prediction from a rotating cylinder in subcritical Reynolds flow *Leonidas Siozos-Rousoulis, Ghader Ghorbaniasl, Chris Lacor*
11:20	An algebraic model for prediction of bypass transition in turbomachinery boundary layer flows *Erik Dick, Slawomir Kubacki*	A Novel EARSM model for separated flows *Stephane Monte, Lionel Temmerman, Benoit Léonard, Benoît Tartinville, Charles Hirsch*	Adaptive LES modeling in the context of discontinuous finite elements methods *Jean-Baptiste Chapelier, Guido Lodato*	Overset LES for Trailing-Edge Noise Computations *Rinie Akkermans, Paul Bernicke, Roland Ewert, Juergen Dierke*
11:40	Laminar-turbulent transition in Hagen-Poiseuille flow of a real gas *Sergey Novopashin, Gennady Sukhinin, Petr Skovorodko*	The development of algebraic stress models using a novel evolutionary algorithm *Jack Weatheritt, Richard Sandberg*	Investigation of various wall modeling approaches for LES in the presence of mild pressure gradients *Olivier Thiry, Matthieu Duponcheel, Grégoire Winckelmans*	Far-field Noise Prediction of a Rod-airfoil Benchmark by IDDES and FW-H analogy *Wenqing Zhu, Zhixiang xiao*
12:00	An investigation of the transition prediction using KDO RANS model *Jinglei Xu, Ding Xu, Yang Zhang, Junqiang Bai*	Explicit algebraic Reynolds stress modelling of flows with large density variation *Igor Grigoriev, Stefan Wallin, Geert Brethouwer, Arne Johansson*	Improved Eddy-Viscosity Modelling of Wind Turbine Wake Interactions *Sasa Kenjeres, Joep Hennen*	A Numerical Study on the Sound Absorption Mechanism of A Non-Locally Reacting Liner under High SPL *Chao Chen, Xiaodong Li, Frank Thiele*
12:20	Further assessment of the grey-area enhanced sigma-DES approach for complex flows *Marian Fuchs, Charles Mockett, Jörn Sesterhenn, Frank Thiele*	A numerically robust Reynolds stress model for improved prediction of practically relevant separating flow applications *Robert Maduta, Suad Jakirlic*	Dynamic global-coefficient procedures for wall-adapting subgrid-scale models *Shahriar Mohammadi, Romuald Skoda*	Direct Numerical Simulation of a Helmholtz resonator excited by a low Mach number turbulent flow *Lewin Stein*
12:40-14:00	**Lunch**			

AN ALGEBRAIC MODEL FOR PREDICTION OF BYPASS AND SEPARATION-INDUCED TRANSITION IN TURBOMACHINERY BOUNDARY LAYER FLOWS

S.Kubacki[1], E.Dick[2]

[1]Institute of Aeronautics and Applied Mechanics, Warsaw University of Technology, Nowowiejska 24, 00-665, Warsaw, Poland
[2]Department of Flow, Heat and Combustion Mechanics, Ghent University, St.–Pietersnieuwstraat 41, 9000 Ghent, Belgium

Slawomir.Kubacki@meil.pw.edu.pl, Erik.Dick@UGent.be

Abstract

An algebraic intermittency model for bypass and separation-induced transition is presented. The transition model modifies the production terms of a k-ω turbulence model. It uses only local variables and is tuned for turbomachinery flows. For bypass transition, two effects in an attached pre-transitional boundary layer are expressed: damping of small-scale disturbances induced by the free stream and breakdown of the near-wall perturbed flow with generation of fine-scale turbulence. For separated flow, the model describes breakdown of a laminar free shear layer. The model is a modified and extended version of an earlier model by the authors for bypass transition only (Kubacki and Dick, 2016).

1 Transition mechanisms

With a turbulence level above 0.5-1 %, the free-stream turbulence induces streamwise elongated disturbances in the near-wall region of an attached laminar boundary layer, termed streaks or Klebanoff modes. These are zones of forward and backward jet-like perturbations, alternating in spanwise direction. Streaks grow downstream both in length and amplitude and finally some streaks cause turbulent spots. Transition is then called of bypass type, which means that instability by Tollmien-Schlichting waves is bypassed. Breakdown is then earlier and much faster. Bypass mechanisms are discussed by Hack and Zaki (2014). Klebanoff modes are initiated by deep penetration into a laminar boundary layer of large-scale perturbations from the free stream. The strong damping of small-scale components is called shear sheltering. There are at least two instability mechanisms in a boundary layer perturbed by streaks. One is instability by inflection of the velocity profile in wall-normal direction between the boundary layer edge and a low-speed streak. The other is instability of the velocity profile in wall-normal direction in the overlap zone of the leading edge of a high-speed streak and the trailing edge of a low-speed streak. Both instabilities are triggered by small-scale perturbations, although these are damped in the boundary layer

In a separated laminar boundary layer, under low free-stream turbulence, transition is initiated by inviscid Kelvin-Helmholtz instability, with formation of spanwise vortices. They group at selective streamwise wavelengths, analogous to Tollmien-Schlichting waves in an attached boundary layer (McAuliffe and Yaras, 2010). The roll-up vortices break down as they travel downstream. The breakdown process is rather slow with low free-stream turbulence, but, under high free-stream turbulence, bypass transition with formation of streaks in the attached boundary layer prior to separation can coexist with the Kelvin-Helmholtz generated spanwise vortices in the separated layer. The breakdown of the vortex rolls is then strongly accelerated by perturbations due to the Klebanoff modes. For sufficiently strong free-stream turbulence, the Kelvin-Helmholtz instability may even be bypassed by the breakdown of the streaks. So, a bypass mechanism is possible in a separated shear layer, similar as in an attached boundary layer.

2 Model formulation

The transport equations for turbulent kinetic energy and specific dissipation rate are

$$\frac{Dk}{Dt} = \gamma P_k + (1-\gamma)P_{sep} - \beta^* k\omega + Diff\,(k), \quad (1)$$

$$\frac{D\omega}{Dt} = \alpha\frac{\omega}{k}P_k - \beta\omega^2 + Diff\,(\omega). \quad (2)$$

The equations are the k-ω equations of the turbulence model of Wilcox (2008), with three modifications in the production terms. In the original model, production of turbulent kinetic energy by turbulent shear is $P_k = \nu_T S^2$, with ν_T the eddy viscosity and $S = (2S_{ij}S_{ij})^{1/2}$ the magnitude of the shear rate tensor. Firstly, this production term is written as $P_k = \nu_s S^2$, where ν_s is the small-scale eddy viscosity, which is part of the full eddy viscosity ν_T. Secondly, in the k-equation, the production term P_k is multiplied with an intermittency factor γ, which is zero in laminar flow and unity in turbulent flow. Thirdly, the term $(1-\gamma)P_{sep}$ is added to the production term of the k-equation.

This term models turbulence production by instability and breakdown of a laminar free shear layer in a low turbulence level background flow.

The turbulent kinetic energy k is split, based on the laminar-fluctuation kinetic energy transition model by Walters and Cokljat (2008), into a small-scale part and a large-scale part:

$$k_s = f_{SS} k, \quad k_\ell = k - k_s . \tag{3}$$

The splitting by the factor f_{SS} expresses the shear-sheltering effect. An attached pre-transitional boundary layer is laminar for a large part near to the wall, but the top part is turbulent. Small-scale disturbances in the turbulent flow near to the laminar part are damped. Only large-scale disturbances penetrate deeply into the laminar part of the layer, but these do not contribute to turbulence production by shear but induce the streaks. The restriction of the turbulence production by turbulent shear to small-scale fluctuations is expressed by replacing the full eddy viscosity by a small-scale eddy viscosity in the production terms of the k- and ω-equations.

Shear-sheltering depends on the ratio of two timescales in a laminar layer: the timescale of convection of disturbances relative to an observer inside the layer and the timescale of diffusion in the normal direction. Walters (2009) estimates the convective time scale by the time scale of the strain, $\tau_c = 1/\Omega$, with Ω the magnitude of the vorticity tensor. The diffusive time scale is fundamentally ℓ^2 / ν, with ℓ the fluctuation length scale in normal direction and ν the kinematic fluid viscosity. Walters (2009) expresses damping of small-scale fluctuations, by stating that fluctuations in the border zone of the laminar and turbulent parts synchronise strongly with the mean velocity gradient in the laminar part. So, he assumes that fluctuations, both in streamwise and in wall-normal direction, after damping, scale with $\ell\Omega$. This means proportionality between $\sqrt{k}$ and $\ell\Omega$, resulting in $\ell \propto \sqrt{k}/\Omega$ and $\tau_d \propto k/(\nu\Omega^2)$. The ratio of the diffusive and convective timescales is the Reynolds number $Re_\Omega = k/(\nu\Omega)$. With the supplementary assumption that in the laminar part of a pre-transitional boundary layer the wall-normal fluctuation length scale is proportional to the distance to the wall, denoted by y, Ω may be eliminated by replacing it by $\sqrt{k}/y$. This means that the characteristic Reynolds number for shear-sheltering may also be $Re_y = \sqrt{k}y/\nu$. We use the shear-sheltering factor of the model by Walters and Cokljat (2008), but by replacing Re_Ω by Re_y, leading to

$$f_{SS} = exp\left(-\left(\frac{C_{SS}\nu}{\sqrt{k}y} \right)^2 \right). \tag{4}$$

$C_{SS} = C_S\left(1 + C_A f_W \psi\right)$ is a flow-dependent coefficient. C_S and C_A are constants. C_A is set to unity while C_S has been determined by simulations of T3C flat plate flows of ERCOFTAC (results are not shown). The ψ and f_W functions are:

$$\psi = tanh\left(\frac{-\Omega(S-\Omega)}{C_\psi \left(\beta^* \omega\right)^2} \right), \; f_W = 1 - tanh\left(\frac{k}{C_W \nu \omega} \right). \tag{5}$$

The role of the flow-dependent term $f_W\psi$ is increasing C_{SS} (larger shear sheltering) in accelerating flow ($f_W\psi > 0$), and reducing C_{SS} (smaller shear sheltering) in decelerating flow ($f_W\psi < 0$), for acceleration or deceleration due to streamline curvature. The ψ function is the curvature sensor from the non-linear eddy-viscosity turbulence model of Khodak and Hirsch (1996). The f_W function limits the correction to the border zone of the laminar and turbulent parts in a pre-transitional boundary layer. The C_W and C_ψ are positive constants**,** determined by simulations of flows through the N3-60 steam turbine cascade and the V103 compressor cascade (results are not shown). We discuss simulations of the N3-60 cascade later.

The eddy viscosity associated to small scales is calculated in the same way as the eddy viscosity of the original turbulence model (Wilcox, 2008) by replacing k by k_s:

$$\nu_s = \frac{k_s}{\tilde{\omega}} \quad with \quad \tilde{\omega} = max\left[\omega, \frac{C_{lim} S}{a_s} \right]. \tag{6}$$

The constant a_s is set to 0.3 and $C_{\mathrm{lim}} = 7/8$, which are the standard values. The large-scale eddy viscosity, is, similarly defined with k_l:

$$\nu_l = \frac{k_s}{\tilde{\omega}} \quad with \quad \tilde{\omega} = max\left[\omega, \frac{C_{lim} S}{a_l} \right]. \tag{7}$$

The constant a_l is set to 0.45, which is larger than the standard value 0.3. The resulting eddy viscosity, used in the Navier-Stokes equations, is $\nu_T = \nu_s + \nu_l$. The reason for the enlarged value of a_l with respect to a_s is earlier transition due to increased instability of a laminar flow perturbed by streaks under an adverse pressure gradient (see our earlier work: Kubacki and Dick, 2016).

The intermittency factor γ determines when a flow region is laminar or turbulent. The free stream is turbulent. Thus γ is set to unity in the free stream. At a wall, the flow is laminar. Hence, γ is set to zero there. γ is prescribed algebraically as a function of the distance to the wall by

$$\gamma = min\left(max\left(\frac{\sqrt{k}y}{A_\gamma \nu} - 1, 0 \right), 1 \right), \tag{8}$$

were A_γ is a constant.

The intermittency function is somewhat simplified with respect to the function of our previous work (Kubacki and Dick, 2016) by equalising the threshold value C_T and the growth rate A_T ($C_T = A_T = A_\gamma$), but

this is not a significant change. A more significant change concerns the shear-sheltering factor (Eq. 4). We used the factor from the model by Walters and Cokljat (2008) with Re_Ω as input parameter in our previous work. Now, we replace Re_Ω by Re_y, such that f_{SS} is now also dependent on the distance to the wall, normalised in the same way as with the intermittency function. This change improves much the correspondence between predictions of the onset of bypass transition by the model and empirical correlations (improved results are not shown; see Figs. 8 and 9 in Kubacki and Dick, 2016, for previous results).

The functioning of the model for bypass transition is identical to that of our previous version (see Fig. 7 in Kubacki and Dick, 2016). The intermittency function (Eq. 8) defines an outer turbulent zone and a near-wall laminar zone in an attached boundary layer. Far upstream of transition onset, the border of the zones is about halfway the boundary layer thickness. The shear-sheltering function (Eq. 4) dampens turbulence in the turbulent zone near the border with the laminar zone. This reduces the penetration of turbulence by diffusion in the laminar part of the boundary layer. As the boundary layer grows, more turbulence enters the laminar part and the border of the laminar and turbulent zones shifts towards the wall. When a critical level of turbulent stress is reached, the speed of shifting of this border increases strongly such that it approaches the wall. This way, breakdown is simulated. Fully turbulent state is obtained when the border of the laminar and turbulent states and the zone of damping of the turbulence both come into the viscous sublayer.

The present model, in contrast to our previous version, includes turbulence production due to breakdown of a laminar separated boundary layer at low free-stream turbulence level using 2D RANS (or 2D/3D URANS). This is realised by addition of the term $(1-\gamma)P_{sep}$ to the production term in the k-equation (Eq. 1). For P_{sep} we adopt a term with the same purpose in the newest intermittency-transport transition model by Menter et al. (2015):

$$P_{sep} = C_{sep} F_{sep} \nu S^2 , \qquad (9)$$

$$F_{sep} = min\left(max\left(\frac{R_V}{2.2 A_V} - 1{,}0 \right), 1 \right), \qquad (10)$$

with $R_V = y^2 S / \nu$. The constants C_{sep} and A_{V} have been calibrated for the T3C4 flat plate flow of ERCOFTAC, which is characterized by laminar boundary layer separation in the rear part of the plate (result are not shown). Table 1 lists the model constants.

Table 1. Transition model constants.

A_γ	C_{S}	C_{A}	C_ψ	C_{W}	C_{sep}	A_{V}	a_1
12.0	21.0	1.0	10.0	6.0	2.0	550.0	0.45

3 Computational aspects

All simulations reported here are for the N3-60 steam turbine cascade using 2D RANS or 2D URANS. The 2D computational grids, with about $1.1 \cdot 10^5$ cells, consist of a structured boundary layer part with quadrilateral cells near to walls and an unstructured part away from walls. The grid is refined near to walls. The y^+ parameter varies between 0.1 and 0.8 along walls and about 40 cells are used across the boundary layer grid part.

4 N3-60 cascade with steady inflow

We discuss the model performance for transition in attached and in laminar separation states by 2D RANS for steady inflow of the N3-60 cascade, measured by Zarzycki and Elsner (2005). The blades of the N3-60 are a scaled stator vane in the high-pressure part of a steam turbine. Geometric data are: blade chord 300 mm, axial blade chord 203.65 mm, blade pitch 240 mm. The exit Reynolds number is $6 \cdot 10^5$. Measurements are available for inflow turbulence Tu = 3% and Tu = 0.4% in the leading edge plane. Laminar separation occurs at the suction side for Tu = 0.4%.

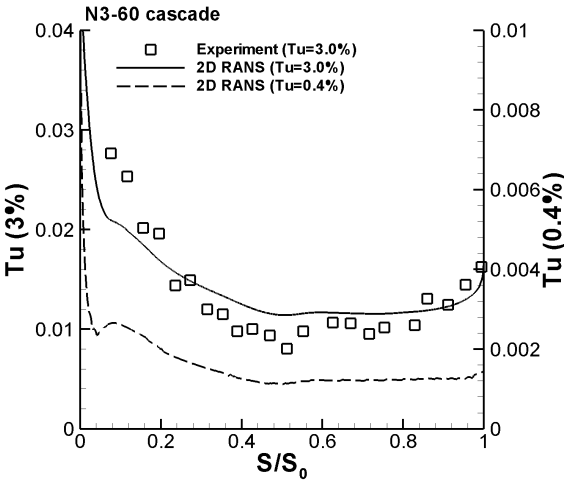

Figure 1: N3-60 cascade. Turbulence intensity along the suction side of the blade at distance 10 mm from the blade surface for Tu = 3 % and Tu = 0.4 %. S_0 is the length of the suction side of the blade.

At the inlet to the computational domain, placed at 0.344 times the axial chord length upstream of the leading edge, a uniform flow velocity in the axial direction was imposed. The inlet turbulence intensity in the leading edge plane was set according to the two sets of experimental data. The inlet turbulent length scale was not reported in the measurements. For Tu = 3 %, the inlet turbulent length scale was adjusted by matching the measured turbulence intensity at a distance of 10 mm from the blade surface (this is above the boundary layer edge). The obtained turbulent length scale is l_t = 9 mm for Tu = 3 %. Fig. 1 shows that the agreement between prediction and measure-

ment is reasonably good, which means that the inlet conditions for the modelled scalars have been set correctly. For low turbulence level at inlet (Tu = 0.4%), the evolution of the free-stream turbulence along the blade surface is not available in the database. We assume a smaller length scale (l_t = 2mm) at the entrance to the cascade than for high inlet turbulence level since no turbulence grid was installed in the experiment. The turbulent intensity reproduced at the leading edge of the blade corresponds with measurements, Tu = 0.5–0.4% (Fig. 1).

Fig. 2 shows the contour plot of turbulent kinetic energy for Tu = 3% and the comparison between computed and measured shape factor H_{12} along the suction side of the blade. The simulated transition comes from the bypass term γP_k in Eq. 1. Transition onset, at S/S_0 = 0.75, and growth rate in the transition zone are reproduced correctly by the model.

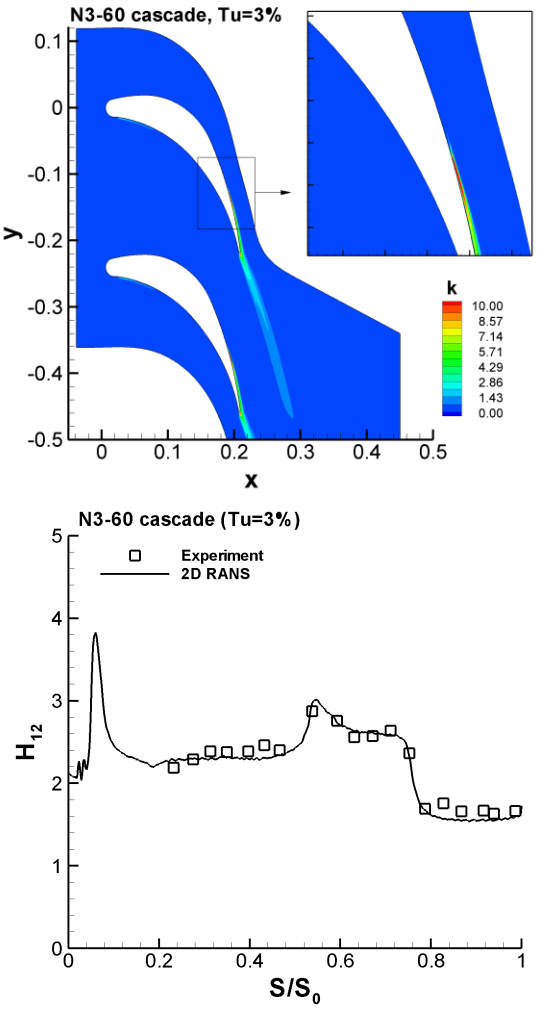

Figure 2: N3-60, Tu = 3%. Turbulent kinetic energy (top) and shape factor along the suction side of the blade (bottom) using 2D RANS.

Fig. 3 shows the contour plot of turbulent kinetic energy for Tu = 0.4% and the comparison between computed and measured shape factor H_{12} along the suction side of the blade. The simulated transition comes here from the separation term $(1-\gamma)P_{sep}$ in Eq. 1. Start of transition is observed at S/S_0 = 0.9. The agreement between simulation and measurement is very good. It means that the model calibration for separation-induced transition by the T3C4 case has been done well. Notice that in the previous model (Kubacki and Dick, 2016) the transition in a separated laminar boundary layer was not modelled, but was resolved using 3D URANS. This is no longer necessary, as transition in a separated boundary layer is fully modelled now.

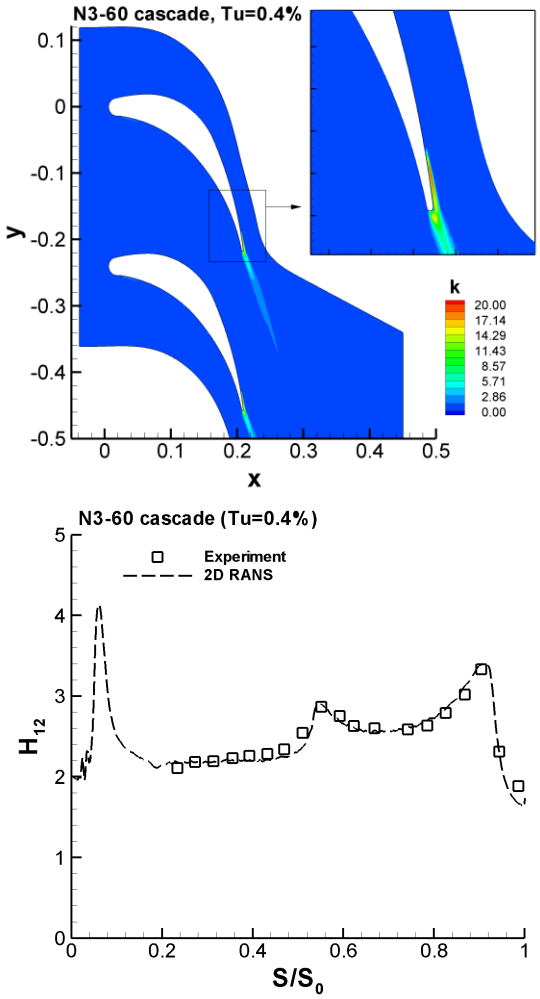

Figure 3: N3-60, Tu = 0.4%. Turbulent kinetic energy (top) and shape factor along the suction side of the blade (bottom) using 2D RANS.

5 N3-60 cascade with unsteady inflow

The final model validation is performed with wake-induced transition for flow through the N3-60 cascade using 2D URANS. Simulation results are compared with measurements by Zarzycki and Elsner (2005). In the experiments the wake generator was a wheel of pitch diameter D_p = 1950 mm with cylindrical bars rotating in a plane perpendicular to the flow direction. The bars were spaced by b_s = 204 mm on the pitch circle. The axial distance between the bars and the leading edge of the blades was 0.344 of the

axial blade chord length. The frequency of the incoming wakes was f_d = 59 Hz, with inflow velocity U_0 = 10 m/s, resulting in the reduced frequency: $St = f_d b_s/U_0 = 1.22$. The exit Reynolds number was $6 \cdot 10^5$. The free-stream turbulence intensity Tu was controlled with a movable grid upstream of the cascade entrance. We use the data for bar diameters d = 6 and 4 mm with inflow turbulence levels Tu = 3 and 0.4 %, respectively. The inlet to the computational domain is placed at 0.17 times the axial chord length upstream of the leading edge. The effect of the moving bars was superimposed on the flow obtained from the steady calculation. The bar pitch has been increased to 240 *mm* to be equal to the blade pitch in the calculation. The bar velocity has been adjusted, so that the reduced frequency (St) of the impacting wakes is unchanged. 800 time steps were used per wake period. Self-similar profiles for velocity and turbulent kinetic energy were imposed at the inlet:

$$U = U_\infty - (U_\infty - U_{center}) exp\left[-(ln\,2)\left(\frac{y}{y_{1/2}} \right)^2 \right] ,$$

$$k = k_\infty + (k_{center} - k_\infty) exp\left[-(ln\,2)\left(\frac{y}{y_{1/2}} \right)^2 \right] . \quad (11)$$

In the above expressions, y is the distance perpendicular to the wake with y = 0 the centre of the wake and $y_{1/2}$ is the position where the defect of the velocity attains half of its maximum value. The parameters in the above expressions have been fitted to experimental data for wakes of stationary bars. The specific dissipation at the inlet was imposed following Wilcox (1993):

$$\omega = \omega_\infty + C_\mu^{1/4} \frac{\sqrt{k}}{l_{mix}} \ , \ l_{mix} = 0.18 y_{1/2} . \quad (12)$$

The background dissipation ω_∞ has been adjusted to reproduce the evolution of the fluctuating velocity component parallel to the blade, $u' = (2k/3)^{1/2}$, at distance 10 mm from the suction surface of the blade to the experimental one for moving bars (results are not shown).

Fig. 4 shows the perturbation velocity vectors in every 15 cells, obtained by subtracting the time-averaged velocity field from the instantaneous velocity field. Clearly, the $1.1 \cdot 10^5$ mesh is sufficient to properly reproduce the negative jet effect caused by a moving wake.

Fig. 5 shows space-time diagrams of shape factor obtained in the experiment (a) and in the simulation (b) for wake-induced transition with background turbulence level Tu = 3 % (d = 6 mm). The two straight lines mark the path of the moving wake. The wake position was determined from the free-stream velocity at the edge of the boundary layer. The bottom line is the path of the leading edge of the wake, determined as the position at which local flow acceleration starts (not shown) in the rear part of the blade (S/S_0 > 0.6). The upper line corresponds to the central part of the moving wake (start of local flow deceleration).

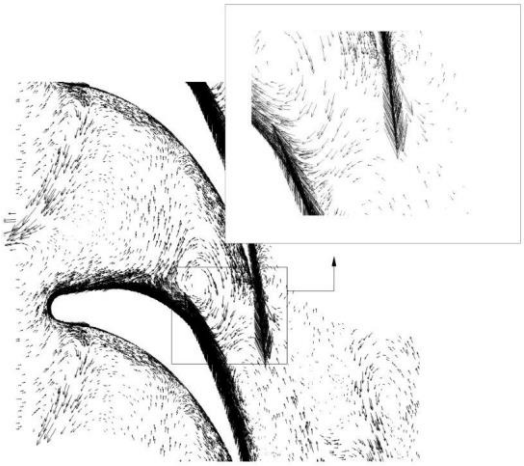

Figure 4: Negative jet visualised by perturbation velocity vectors in every 15 cells for 2D URANS.

The agreement between simulation and measurement is very good under the wake impact (S/S_0 = 0.6, τ/T = 0.2). The width of the turbulent zone is somewhat too large at S/S_0 = 0.7−0.8 and the transition is reproduced somewhat too late in between wakes near to the trailing edge (S/S_0 = 0.9, 1.0 < τ/T < 1.2).

Fig. 6 shows space-time diagrams of shape factor for wake-induced transition with background turbulence level Tu = 0.4 % (d = 4 mm). The model is able to properly detect transition onset under the wake impact (S/S_0 = 0.7, τ/T = 0.4). The width of the turbulent zone, after wake impact, is comparable in simulation and measurement. The quality of the model becomes less in between wakes (S/S_0 = 0.9, 1.1 < τ/T < 1.5) near to the trailing edge of the blade. The model predicts flow separation, which is not present in the experiment. The explanation is the somewhat too low free-stream turbulence level reproduced in the simulation in the rear part of the blade, which causes delayed transition there. In the experiment, interaction occurs near the suction side trailing edge between the wake of the adjacent blade and the moving wake through the blade passage. Vortices are shed from the blade wake, which beak down, causing increased free-stream turbulence, This interaction is not detected in the 2D URANS simulation.

Overall, the simulation results of wake-induced transition both at high (Tu = 3%) and low (Tu = 0.4%) background turbulence levels are good using the present algebraic transition model.

6 Conclusion

An algebraic intermittency model has been presented. The model produces good results for bypass and separation-induced transition (2D RANS) and for wake-induced transition (2D URANS), for flow through the stream turbine vane cascade N3-60, at both high and low free-stream turbulence levels.

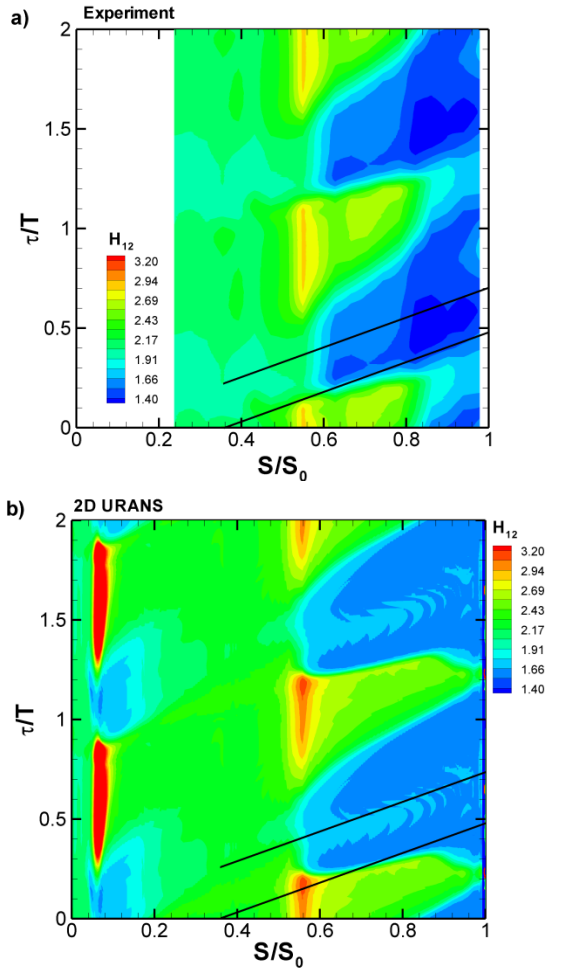

Figure 5: N3-60 cascade, bar diameter 6 mm and background turbulence level 3 %. Space-time diagrams of shape factor, a) experiment, b) simulation.

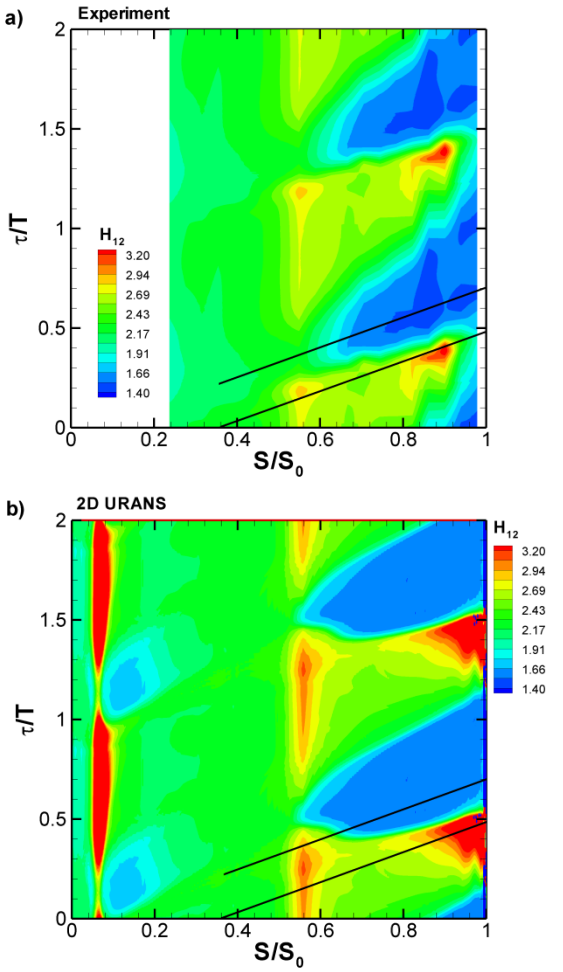

Figure 6: N3-60 cascade, bar diameter 4 mm and background turbulence level 0.4 %. Space-time diagrams of shape factor, a) experiment, b) simulation.

Acknowledgements

The first author acknowledges support from the research project COOPERNIK financed partly by the Polish National Centre for Research and Development (INNOLOT/I/11/NCBR/2014) and partly by Avio Polska Sp. z o.o.

References

Hack M.J.P., Zaki T.A. (2014), Streak instabilities in boundary layers beneath free-stream turbulence, *J. Fluid Mech.*, 741, 280-315.

Khodak A., Hirsch C. (1996), Second-order non-linear k-ε models with explicit effect of curvature and rotation, in *Proceedings of Third ECCOMAS Computational Fluid Dynamics Conference, Paris, France*, Wiley, ISBN 0471958514, 690-696.

Kubacki S., Dick E. (2016), An algebraic model for bypass transition in turbomachinery boundary layer flows, *Int. J. Heat and Fluid Flow*, 58, 68-83.

McAuliffe B.R., Yaras M.I. (2010), Transition mechanisms in separation bubbles under low- and elevated freestream turbulence, *J. Turbomachinery*, 132, 011004/1-10.

Menter F.R., Smirnov P.E., Liu T., Avancha R. (2015), A one-equation local correlation-based transition model, *Flow Turbul. Combust.*, 95, 583-619.

Walters. K. (2009), Physical interpretation of transition-sensitive RANS models employing the laminar kinetic energy concept, *Ercoftac Bulletin*, 80, 67-76.

Walters D.K., Cokljat D. (2008), A three-equation eddy-viscosity model for Reynolds-averaged Navier-Stokes simulations of transitional flow, *J. Fluids Engineering*, 130, 121401/1-14.

Wilcox D.C. (1993), Turbulence modelling for CFD. DCW Industries, Inc.

Wilcox D.C. (2008), Formulation of the k-ω turbulence model revisited. *AIAA J.*, 46, 2823-2837.

Zarzycki R., Elsner W. (2005), The effect of wake parameters on the transitional boundary layer on a turbine blade, *IMechE Part A, J. Power and Energy*, 219, 471-480.